A Hybrid FMCW-Interferometry Radar for Indoor Precise Positioning and Versatile Life Activity Monitoring

Guochao Wang, *Student Member, IEEE*, Changzhan Gu, *Member, IEEE*, Takao Inoue, *Member, IEEE*, and Changzhi Li, *Senior Member, IEEE*

***Abstract*—This paper presents a hybrid radar system that incorporates a linear frequency-modulated continuous-wave (FMCW) mode and an interferometry mode for indoor human localization and life activity monitoring applications. The unique operating principle and signal processing method allow the radar to work at two different modes for different purposes. The FMCW mode is responsible for range detection while the interferometry mode is responsible for life activities (respiration, heart beat, body motion, and gesture) monitoring. Such cooperation is built on each mode's own strength. Beam scanning is employed to determine azimuth information, which enables the system to plot 360° 2-D maps on which the room layout and objects' location can be clearly identified. Additionally, the transmitted chirp signal is coherent in phase, which is very sensitive to physiological motion and allows the proposed technique to distinguish human from nearby stationary clutters even when the human subjects are sitting still. Hence, the proposed radar is able to continuously track the location of individuals and monitor their life activities regardless of the complex indoor environment. A series of experiments have been carried out to demonstrate the proposed versatile life activity monitoring system.**

***Index Terms*—Frequency modulated continuous wave (FMCW), interferometry, life activities, stationary clutter removal, 2-D positioning, vital sign monitoring.**

I. Introduction

INDOOR short-range high-accuracy radar sensors can serve as an important cyber chamberlain that provides a cozy home environment with thoughtful services including, but not limited to: 1) positioning and navigation; 2) home security; 3) remote real-time health care; 4) wireless user interface (UI); and 5) entertainment based on fully non-contact body gaming. Currently these applications are mainly carried out by contact sensors such as transducers and/or optical image sensors. In most cases, especially for long-term health care, people are reluctant to wear contact sensors all the time, which limits the applications of contact sensors mainly to emergency usage. For optic-based techniques such as a closed-circuit television (CCTV) and infrared camera, they have been widely used in homeland security and surveillance. The recent advancement in optical video such as Kinect can provide an accurate depth image and draw magnificent interests from many areas [1]. Despite the great success they have achieved, optic-based techniques still suffer from several tough problems. Although video can provide pictures with volume and detailed data, it is not good at revealing tiny vital sign information due to the inadequate image resolution. Additionally, optical sensors can be easily blocked by obstacles between the target and sensors, and hence require direct exposure and suffer from a blind zone problem. On the contrary, non-contact microwave radar sensors have advantages over other alternatives. First, microwave radar is more sensitive in tiny vital signs [2], [3] because it can provide millimeter or even sub-millimeter scale accuracy [4], [5]. Second, microwave sensors do not rely on light and can penetrate walls and obstacles [6], [7]. Third, the Doppler and micro-Doppler characteristics reveal extra details of motion, and thus enable gesture recognition [8].

However, there are still some limitations for the current microwave radar sensor to fully handle real-time individual life activities. The greatest challenge for the microwave radar sensor is how to provide sufficient range detection and displacement monitoring accuracy at a low cost. There are several mainstream radar architectures that can be found in the literature, i.e., Doppler (interferometry) radars [9]–[11], impulse-radio ultra-wideband (IR-UWB) radars [3], [6], [12]–[14], frequency-modulated continuous-wave (FMCW) radar [15]–[19] and stepped frequency-modulated continuous-wave (SFCW) radar [20]. Doppler radars operate based on single-tone continuous wave (CW) to obtain phase history. They have been widely used because of their high precision in displacement measurement. However, they can hardly detect range information. Although multiple Doppler radars cooperating with the arrival of angle (AOA) algorithm can estimate the position of moving targets [21], the challenge for a single Doppler radar to spatially distinguish multiple targets limits the application of traditional indoor Doppler radar sensors mainly to vital sign monitoring and gesture recognition. IR-UWB, FMCW, and SFCW radars are capable of providing range information.

Manuscript received March 19, 2014; revised June 07, 2014 and August 02, 2014; accepted September 08, 2014. Date of publication September 23, 2014; date of current version November 03, 2014. This work was supported in part by the National Science Foundation (NSF) under Grant ECCS-1254838 and Grant CMMI-1131506 and in part by National Instruments.

G. Wang and C. Li are with the Department of Electrical and Computer Engineering, Texas Tech University, Lubbock, TX 79409 USA (e-mail: guochao.wang@ttu.edu; changzhi.li@ttu.edu).

C. Gu is with Marvell Semiconductor Inc., Santa Clara, CA 95054 USA (e-mail: cgu@marvell.com).

T. Inoue is with National Instruments, Austin, TX 78759 USA (e-mail: takao.inoue@ni.com).

Color versions of one or more of the figures in this paper are available online at http://ieeexplore.ieee.org.

Digital Object Identifier 10.1109/TMTT.2014.2358572

However, their range resolution is highly dependent on the bandwidth transmitted, forcing most of the systems to work at high frequencies for the resolution required by life activities monitoring. Great efforts must be made to overcome the problems associated with high frequency and wide bandwidth (e.g., linearity and frequency drift problems), not to mention the high cost, complexity, and high attenuation it suffers.

In this paper, a novel radar system is presented for precise 2-D positioning and life activities surveillance. Operating in the 5.8-GHz indusrial–scientific–medical (ISM) band with a 160-MHz bandwidth, the radar system incorporates the FMCW mode and the interferometry mode based on a CWform. The FMCW mode is responsible for range detection while the interferometry mode is for tiny physiological motion monitoring. Such a strategy is devised because FMCW can provide range information and interferometry radar is advantageous in relative displacement (e.g., physiological motion) detection. Moreover, they can share the same RF front end because they are both based on CW operation. To achieve high isolation, the TX and RX antennas were separated and both of them have a high gain and low sidelobe. Mechanical antenna rotation was employed to acquire the azimuth information. Thus, the proposed radar system is capable of scanning 360° with an angular step size of 5.625° to locate objects.

The challenge of the proposed application is to differentiate human from stationary clutters, especially when people remains relatively stationary (e.g., when reading, watching TV, or sleeping). In these cases, without the range history information, it is difficult to locate people's position since they remains in a certain range bin just as stationary clutters do. In this paper, differentiating human from surrounding stationary clutters is realized by the cooperation of the FMCW mode and the interferometry mode. Interferometry mode is to quickly determine the azimuth direction of human. When there are both human and clutters along the same line-of-sight (LOS), the coherent chirp signal employed in this paper can distinguish human from clutters based on tiny change in phase history. Therefore, the proposed radar system is fully capable of locating people and monitoring their life activities with decent accuracy. Additionally, possessing high accuracy in Doppler information enables the proposed radar system to recognize a human's gestures and to provide a non-contact interface between people and devices.

This paper is organized as follows. Section II presents the operating principle of the proposed hybrid radar and its subsystems with simulations. In Section III, extensive experiments are carried out to verify the performance in the context of indoor precise positioning and life activity monitoring. A conclusion is drawn in Section IV.

II. Theory

A. Waveform Design and Separation

Fig. 1 shows the proposed transmitted signal and its single point reflected signal in the frequency domain [see Fig. 1(a)] and time domain [see Fig. 1(b)], respectively. The spectrum of the transmitted hybrid signal can be found in [23]. In the time domain, the FMCW signal has the same amplitude as that of

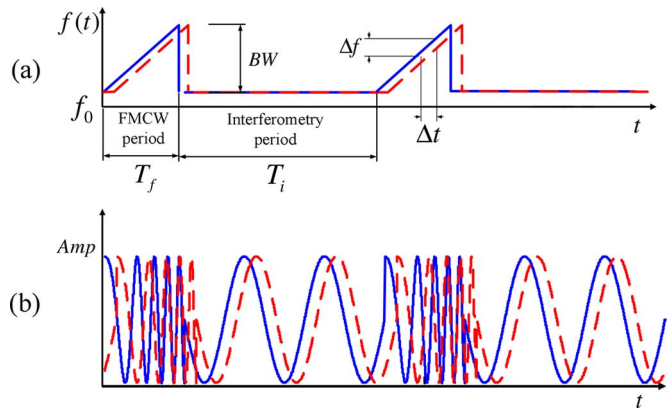

Fig. 1. Proposed hybrid transmitted (solid line) and received signals (dashed line) in the: (a) frequency domain and (b) time domain.

the interferometry signal. Basically, the proposed modulated signal is a sequence of chirp period embedded into single-tone interferometry signal. Therefore, the system is a time division (TD) system that switches between the FMCW mode and interferometry mode. The FMCW signal (chirp signal) is an up-ramp linear frequency-modulated signal, while the interferometry signal has a fixed operating frequency. The duration time of the chirp signal and the interferometry signal are T_f and T_i, respectively. By mixing a local copy of the transmitted signal with the received signal backscattered by the target, the baseband signal contains a series of the FMCW baseband signal and interferometry baseband signal. Simulation results are presented to explain the operating principles. All simulations share the same system parameters, which are exactly the same to the real experiment: operating frequency ranges from 5.72 to 5.88 GHz, $T_f = 2$ ms, $T_i = 98$ ms. A simulated time-domain baseband output when detecting a target located 2 m away from the radar is shown in Fig. 2(a) and (b). To distinguish the two types of baseband signal, in this paper the baseband output during the FMCW period is called the *beat signal* because it contains the beat frequency, and the baseband output during the interferometry period is called the *interferometry signal*.

The beat signal and interferometry signal alternately show up at the receiver baseband output. Therefore, the first step of signal processing is to extract integral beat signals and rebuild the interferometry signal, which are used to provide range information and displacement information, respectively. As shown in Fig. 2(b), the variation of the interferometry signal is much slower than that of the beat signal. This is the basis to isolate the beat signal from the interferometry signal: a sliding window with a length of T_f (same size as a beat signal duration) is applied to calculate the standard deviation of baseband output in that window. The position of the largest sliding window corresponds to the location of the beat signal. This procedure is only taken once to find the first beat signal. Based on the location of the first beat signal and the total time interval $T_i + T_f$ between two adjacent beat signals, the rest of the beat signals can be easily located. It should be noted that strict clock synchronization is necessary between the signal generator, the digitizer, and the baseband signal processor. Otherwise the difference between two clock rates will accumulate and eventually misalign the actual location of the following beat signals.

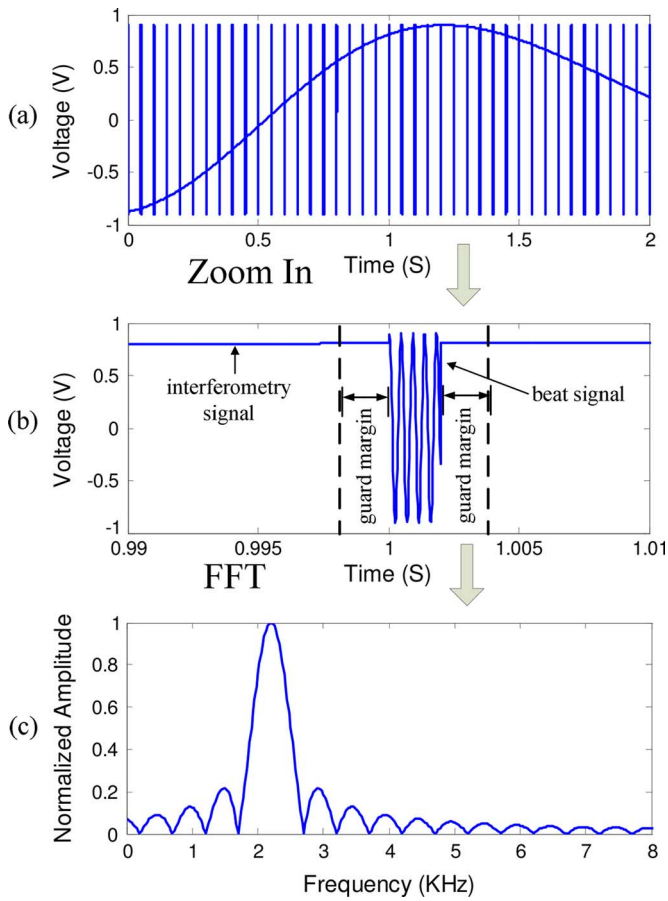

Fig. 2. Procedure of beat signal extraction and beat frequency calculation. (a) Time-domain baseband signal. (b) Zoom-in of the time-domain signal with only one burst of beat signal. (c) Frequency-domain information of the extracted beat signal.

B. Range Information From Extracted Beat Signal

The transmitted complex signal for one chirp period can be expressed as

$$S_T(t) = \exp(j(2\pi f_c t + \pi\gamma t^2 + \phi)) \tag{1}$$

where $\gamma = BW/T_f$ is the chirp rate, t is the so-called fast-time, and ϕ is the initial phase. Keep in mind that the waveform is designed so that the chirp signal is phase coherent so ϕ is a constant.

Intuitively, the received chirp signal lags behind the transmitted signal with the round-trip time-of-flight (RTTOF). Suppose a point scatterer whose distance to the radar is $R(\tau)$, where τ is slow time. Since T_f is very short compared with the target movement speed, it is safe to assume $R(\tau)$ is a constant during each period of the transmitted chirp. The received signal for one point scatterer at $R(\tau)$ is thus given by

$$S_R(t) = \sigma S_T\left(t - \frac{2R(\tau)}{c}\right) \tag{2}$$

where σ is the amplitude of the received signal normalized to the transmitted signal. The mixing of a replica of the transmitted signal with the received one is known as "de-chirping," and results in the beat signal that can be mathematically expressed as

$$\begin{aligned} S_b(t) &= S_{T(t)} \times S_R^*(t) \\ &= \sigma \exp(j(f_b t + p_b + \varphi)) \end{aligned} \tag{3}$$

$$f_b = \frac{2\gamma R(\tau)}{c} \tag{4}$$

$$p_b = \frac{2\pi R(\tau)}{c} \tag{5}$$

where f_b is the beat frequency that is proportional to the distance information, p_b is the slow-time phase history, and φ is the residual phase.

For indoor positioning application, the RTTOF is small. Hence, the received signal and the replica of the transmitted signal arrive at the down-converter almost simultaneously. As shown in Fig. 2(a), the beat signals occur with a fixed interval. Therefore, once the location of one beat signal is determined, those of the following beat signals can be easily predicted based on the FMCW burst interval. Guard margins are employed before and after the beat signal to make sure an integral beat signal waveform can be recovered. The beat signal extraction procedure is shown in Fig. 2. Although the margins belong to interferometry baseband signal, they are short and almost flat, and thus create negligible error to the beat frequency detection. Fig. 2(c) shows the range spectrum of the extracted beat signal.

The extracted I/Q beat signals will be combined together to get a complex signal before applying the fast Fourier transform (FFT). Since this work can easily extract beat signals from the hybrid output, it applies the FFT to a single beat signal padded with zeros. Although the padded zeros do not contribute to extra spectrum resolution, the total number of spectrum samples is increased, alleviating the fence effect and resulting in high detection precision [22]. However, because of the limited bandwidth (e.g., 160 MHz with 5.8-GHz carrier frequency), the range resolution of the FMCW radar still cannot meet the requirement of life activities monitoring (e.g., detection of breathing and heartbeat signals). To solve this challenge, the interferometry signal will be utilized to obtain displacement information.

C. Displacement Information From Interferometry Signal

The normalized interferometry-baseband signal of a point scatterer in baseband I/Q channels can be represented as [2]

$$B_I = \sin\left[\frac{4\pi r(\tau)}{\lambda} + \theta + \Delta\phi(\tau)\right] + \mathrm{DC}_I \tag{6}$$

$$B_Q = \cos\left[\frac{4\pi r(\tau)}{\lambda} + \theta + \Delta\phi(\tau)\right] + \mathrm{DC}_Q \tag{7}$$

where $\lambda = c/f_c$ is the wavelength of the RF carrier, $r(\tau)$ is the displacement of the target in the slow-time domain, θ is a constant residual phase related to the initial distance of the target, $\Delta\phi(\tau)$ is the circuit phase noise, and DC_I and DC_Q are the dc levels of the I/Q channels, respectively. It should be noted that the movement $r(\tau)$ is phase modulated in the cosine and sine trigonometric functions. Therefore, phase demodulation is necessary to recover the phase, and thus movement $r(\tau)$

$$r(\tau) = \tan^{-1}\left(\frac{B_I(\tau) - \mathrm{DC}_I}{B_Q(\tau) - \mathrm{DC}_Q}\right) \cdot \lambda/(4\pi). \tag{8}$$

This is known as arctangent demodulation and is widely employed in interferometry radar due to its robustness to the null point detection issue.

It can be observed from (6) and (7) that the phase change is proportional to $r(\tau)/\lambda$. For the 5.8-GHz signal, a small movement can result in significant phase change that can be easily measured. This makes interferometry radar very sensitive and robust in small movement detection. The drawback of this technique is that it possesses no range information because the phase is periodic.

The periodicity of phase restricts (8) to a range of $[-\pi/2\pi/2] \times (\lambda/4\pi)$. When displacement exceeds this range, a phase unwrapping procedure is necessary to rebuild the actual displacement. The phase unwrapping process is a memory algorithm. Hence, the inserted beat signal cannot be simply ignored even though their duration time only occupies a very small portion of the entire transmitted waveform. Otherwise, the inserted beat signal will severely destroy the phase history. In the previous paper [23], the beat signal eliminating procedure was achieved by a high-order finite impulse response (FIR) filter. The satisfactory filter is costly because it requires a very high sampling rate as well as a high filter order, thus demanding a lengthy computing time. In this paper, an alternative way that is more robust and less resource consuming is implemented. Given that the positions of the beat signals can be easily determined, and the interferometry signal is almost flat within such a short period, it is safe to replace the beat signal with linear interpolation without introducing significant distortion to the interferometry signal. The interferometry signal reconstruction procedure is depicted in Fig. 3. Fig. 3(c) is the rebuilt interferometry signal without FMCW bursts, which can be used for demodulation of the displacement information.

D. 2-D Detection and Target Differentiation

As mentioned in Section I, angular information is obtained by steering the antenna beam. Combing the distance information and the angular information, a 2-D polar coordinate can be constructed, which shows the top view of the objects' locations in a room.

Unlike the optical sensors that can provide detailed information of each object and distinguish them through image processing, it is hard for pure FMCW radar to distinguish people from other objects just using the 2-D top view. In this work, target recognition is realized by the coherent phase property of the chirp signals. In multiple objects circumstance, the beat signal can be represented as

$$S_B = \exp\left(f_b t + \frac{4\pi f_c R(\tau)}{c}\right) + \sum_{i=1}^{N} A_i \exp\left(f_{bi} t + \frac{4\pi f_c R_i}{c}\right) \quad (9)$$

where the first term indicates the normalized beat signal of a moving target if there is any, and the second summation term indicates reflection from stationary clutters; A_i is the relative signal amplitude of the i_{th} clutter compared with that of the target. The transmitted FMCW signal in this paper is designed to be coherent chirps, which means not only the frequencies, but also the initial phases of the chirps are the same [24]. This ensures the signals reflected by stationary clutters are identical from chirp to chirp. For the moving target, however, even if the beat frequencies remain the same, the phase information does not because of the phase change due to the target motion. Ideally, the difference between two beat signals is only related to the moving target

$$S_B(\tau) - S_B(\tau + \Delta\tau) = \exp\left(f_b t + \frac{4\pi f_c R(\tau)}{c}\right) - \exp\left(f_b t + \frac{4\pi f_c R(\tau + \Delta\tau)}{c}\right) \quad (10)$$

Since the FFT operator is a linear operator

$$\text{FFT}[S_B(\tau) - S_B(\tau + \Delta\tau)] = \text{FFT}[S_B(\tau)] - \text{FFT}[S_B(\tau + \Delta\tau)] \quad (11)$$

stationary clutters can also be removed in the subtracted spectrum between different beat signals.

Fig. 4 demonstrates the aforementioned clutter removal procedure. Fig. 4(a) shows two beat signals when detecting a stationary clutter and a moving target at two different time intervals. The target and the clutter are located at 2 and 5 m from the radar, respectively. Their corresponding normalized range spectra are plotted in Fig. 4(b). Since the motion amplitude of the moving target is no greater than 1 cm, its corresponding beat

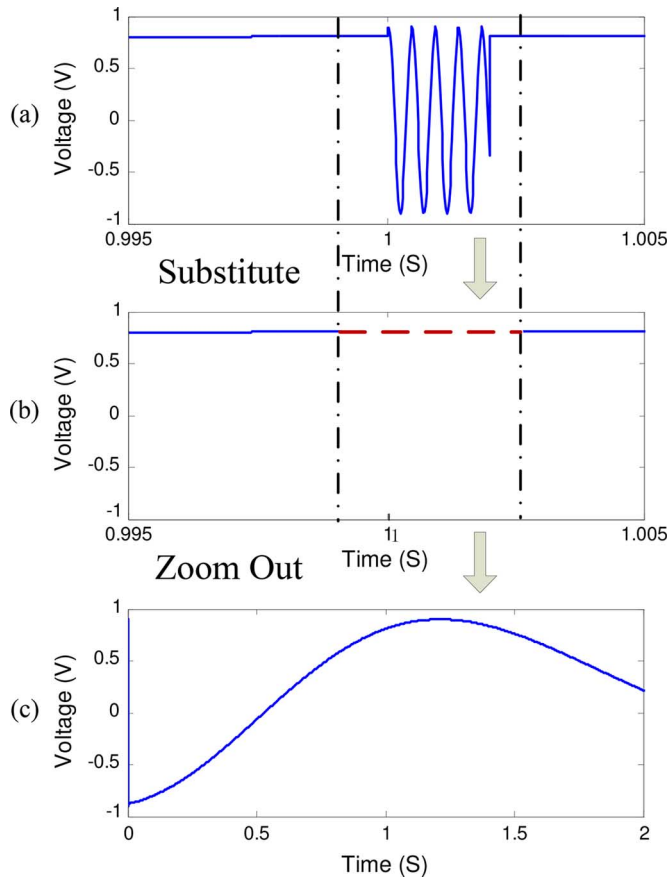

Fig. 3. Procedure to recover interferometry signal. (a) Locate each beat signal period. (b) Replace the beat signal with linear interpolation. (c) Rebuilt interferometry signal.

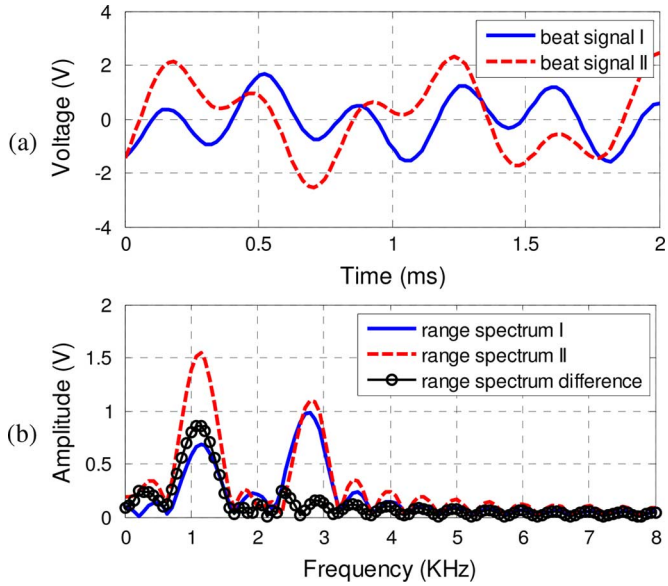

Fig. 4. (a) Two different beat signals at different times. (b) Range spectra of the two beat signals and their difference.

frequency (peak A) is almost unchanged. However, due to summation of scattering from multiple points on the moving target, peak A (target) has a much larger variation in amplitude than peak B (stationary clutter), and the difference between the two range spectra only preserves the information corresponding to the moving target.

E. Micro-Doppler Detection for Motion Classification

Human behavior is more than just respiration or heartbeat. The micro-Doppler has been reported as a signature to distinguish among various life activities [6], [20] and gestures [8], [25], enabling a more comprehensive health-care system and a wireless approach to human–computer interaction. Being sensitive to Doppler effect, interferometry is an ideal technique to monitor the micro-Doppler effect. Its capability in life activities recognition will be demonstrated in this paper. First, the rebuilt interferometry I and Q signals shown in (6) and (7) are combined to obtain the complex signal. With a sliding window, short-time FFT (STFT) can be used to extract the micro-Doppler features.

F. Complete Operation Flow

The complete signal processing flow is shown in Fig. 5. Range information and relative displacement are obtained simultaneously. Notice that the clutter removal algorithm is resource consuming and does not need to be performed at all times. To minimize the computation load, the interferometry mode is employed at the first place to determine the angular direction of the human targets. Since the interferometry mode is more sensitive to tiny movement, if no movement is detected by the interferometry mode at one angular bin, it is safe to assume all the objects in this direction are stationary clutters. In realistic applications to locate human beings, the FMCW mode and the clutter removal process will only be activated when the interferometry mode confirms the existence of a moving target in that direction.

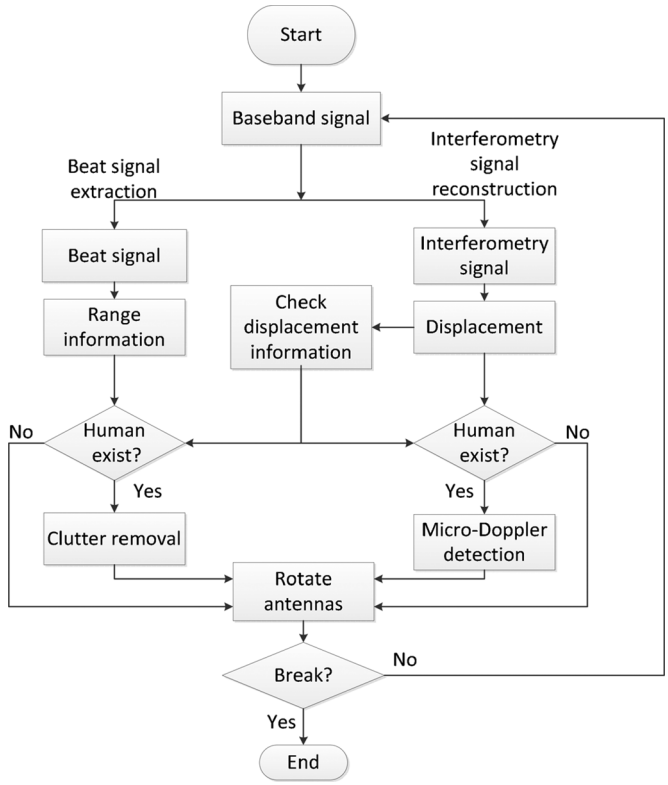

Fig. 5. Baseband signal processing flow.

III. Experimental Results

The hardware and experimental setup of the proposed hybrid radar system are shown in Fig. 6. Fig. 6(a) is the photograph of the prototype system, whose block diagram is also included in Fig. 6(c). The PXIe 5450 is able to export its clock to serve as the reference clock of the ADC (NI cDAQ-9178), which is shown in Fig. 6(b). In this way, the transmitter and receiver are synchronized. The radar system mainly contains three parts: the radar waveform generator, the microwave front end, and the baseband signal processing unit.

The transmitted signal is generated by a National Instruments PXIe 1075 chassis with three function blocks. Follow the signal generation sequence, they are the PXIe 5450 (programmable baseband vector signal generator that can precisely define both the frequency and phase for coherent FMCW signal), the PXIe 5611/PXIe 5652 (up-converter associated with local oscillator), and the PXIe 5691 (variable RF gain block). The final output of the PXIe chassis is a series of FMCW chirp signals embedded in a single-tone CW signal. The linear frequency-modulated chirp signal sweeps from 5.72 to 5.88 GHz with a duration time of 2 ms and a power level of 13 dBm. The interferometry signal has an operating frequency of 5.72 GHz. It is worth mentioning that the PXIe system can also function as a highly accurate interferometry radar when the PXIe 5450 only generates a single-tone signal [26].

Both the FMCW mode and the interferometry mode need a replica of the transmitted signal as the local oscillator to down convert the received signal to derive the beat frequency and Doppler information. The hardware similarity allows the two modes to share the same RF front end. The transmitted signal is split into two by a Wilkinson Power divider. One serves as

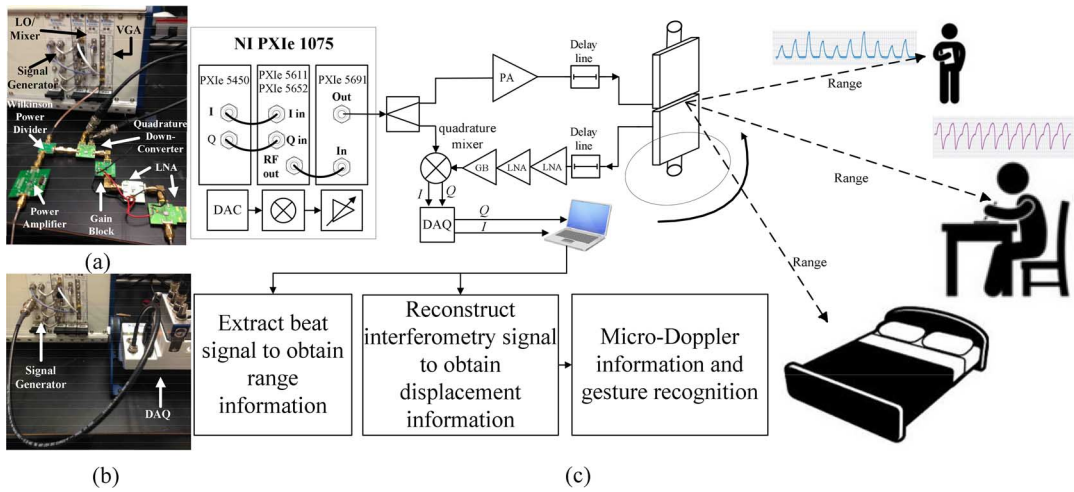

Fig. 6. (a) Photography of the developed hardware system. (b) Synchronization between the signal generator and DAQ. (c) Block diagram of prototype radar system and experimental setup.

the local oscillator and the other is fed into a power amplifier with 17-dB gain to compensate for the free-space loss. On the receiver end, two low-noise amplifiers (LNAs) followed by a gain block amplify the weak received signal with a total gain of 47.5 dB. The last stage of the RF front-end is a quadrature down-converter, where the received signal is mixed with a local copy of the transmitted signal. The I/Q outputs are digitized by an NI 9234 with a consistent 51.2-kHz sampling rate for digital signal processing. To minimize the coupling between the transmitter and the receiver, which is a serious problem for many CW radars, two antennas are employed although it increases the size of the RF front end. Both the TX and the RX antennas have a gain of 17 dBi in the horizontal plane (E-plane) and 14 dBi in the vertical plane (H-plane). Antennas can rotate mechanically in the horizontal plane, and the two antennas were vertically placed up and down to align their radiation beam, as shown in Fig. 6.

For indoor range detection, the objects are close to the radar. Therefore, the RTTOF and its corresponding beat frequencies are small. When the period of the beat signal is comparable to the FMCW duration time, spectrum leakage is severe so that it is hard to get the correct beat frequency. To alleviate this problem, two delay lines were inserted between the antennas and amplifiers at both the transmitter and the receiver sides to increase the delay time and consequently result in a higher beat frequency. Another benefit of a boosting the beat frequency is to minimize the influence of flicker noise in the down-converter. The extra delay introduced by the delay lines and circuit elements is constant and can be easily calibrated as long as the circuit and transmit signal remain the same.

A. Range and Displacement Detection Performance

First, a set of experiments was carried out to evaluate the performance of the proposed hybrid radar system before the indoor 2-D positioning and life activates monitoring experiments.

To evaluate the range detection performance, a cart carrying a piece of metal plate was moving along a ruler from 3 ft (91.44 cm) to 14 ft (426.72 cm) with a step size of 6 in (15.24 cm). Calibration was performed when the target was 5 ft (152.40 cm) away from the antenna. The detected beat frequencies were compared with the calibration beat frequency and the difference in beat frequencies should be linearly proportional to the difference in range. Fig. 7 shows the normalized range spectra at 3, 8, and 13 ft, respectively. In the case of 3-ft distance, the TX-to-RX coupling and clutter are overwhelmed by the strong reflected signal from the target. The complete detected beat frequencies and the corresponding ranges at different locations are shown in Table I. Listed in the fourth column is the standard error from the reference distance measured by the ruler. The maximum error is less than 8 cm and the relative error is below 3%. The error is mainly due to the limited bandwidth and strong nearby clutter interference. The latter dominates when the target was far away from the radar. As the reflected signal strength decreases, the corresponding beat frequency fades and becomes vulnerable to nearby clutter, and may even be overwhelmed by the nearby clutters. Moreover, statistic measurements based on 18 independent distance detection accuracy tests were carried out. Each test repeated the above experiment with actual detection distance ranging from 3 to 12 ft. Fig. 7(d) illustrates the error of the 18 independent tests at 19 different distances. Fig. 7(e) plots the error distribution projected on a 2-D graph. Since the errors are consistent from test to test, the 18 traces overlap with each other at most of the distances. As shown in the figure, the maximum error for all the tests is about 10 cm. The distance detection accuracy is sufficient for most of indoor localization purposes. However, it is still insufficient to detect tiny motion such as respiration or to recognize human gestures.

To evaluate the performance of the proposed radar system when monitoring tiny motions, a metal plate carried by a shaker that can provide programmable sinusoidal motion was employed as the target. During the experiment, the peak-to-peak amplitude and frequency of the shaker were set as 1.5 cm and 0.25 Hz, respectively. The target was placed 1.27 m in front of the radar. The plot in Fig. 8 is the comparison between the radar-detected movement and a reliable reference. The error is less than 1 mm, which is sufficient to tell the detailed information of human activities.

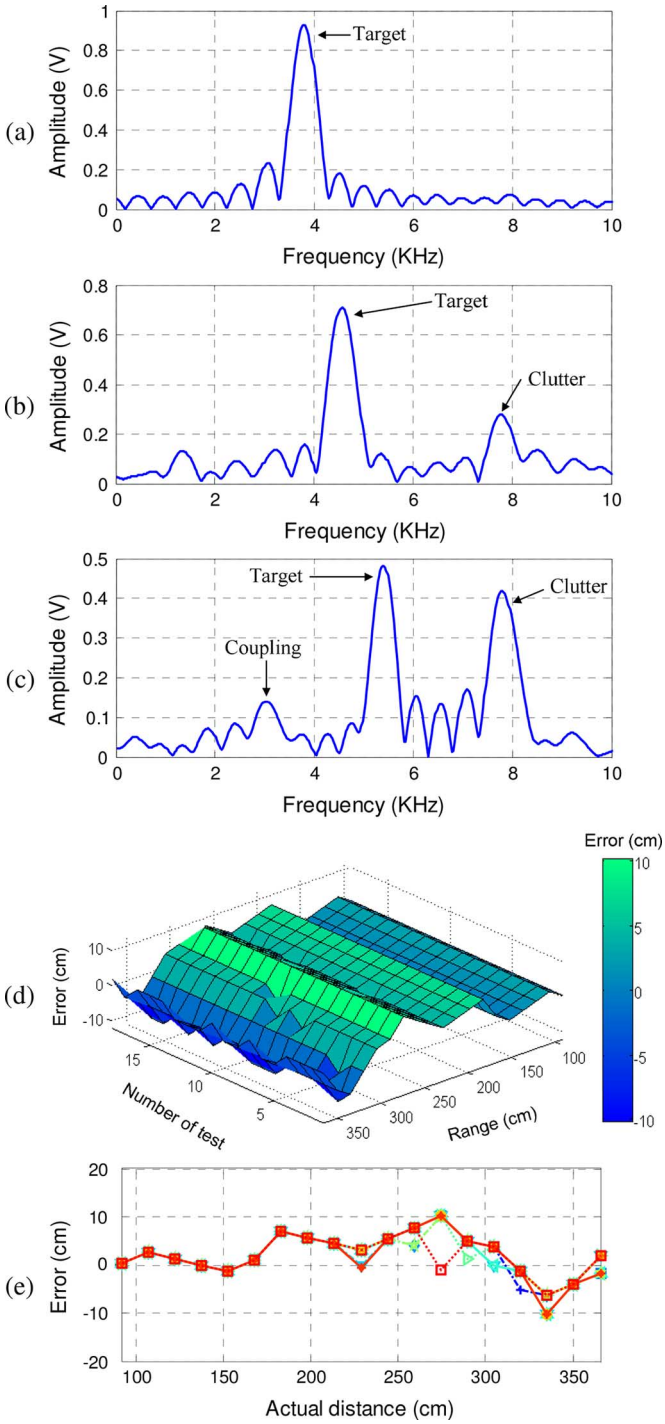

Fig. 7. Range spectra when the target is at: (a) 3 ft, (b) 8 ft, and (c) 13 ft from the radar. (d) Statistic measurement of distance detection error of 18 independent tests. (e) Error distribution of 18 independent tests projected on a 2-D graph.

TABLE I
PERFORMANCE OF ABSOLUTE DISTANCE DETECTION

Reference distance (Feet/cm)	Beat Freq. (Hz)	Measured distance (cm)	Standard error (cm)
3.0/91.44	3793.5	84.84	-6.60
3.5/106.68	3866.0	101.73	-4.95
4.0/121.92	3914.3	120.68	-1.24
4.5/137.16	4010.9	135.51	-1.65
5.0/152.40	4083.4	152.40	0.00
5.5/167.64	4131.8	173.79	6.15
6.0/182.88	4228.4	186.11	3.23
6.5/198.12	4349.2	193.92	-4.20
7.0/213.36	4397.5	215.35	1.99
7.5/228.60	4445.9	236.76	8.16
8.0/243.84	4566.7	244.59	0.75
8.5/259.08	4687.5	252.42	-6.66
9.0/274.32	4711.0	270.07	-4.25
9.5/289.56	4832.5	286.19	-3.37
10.0/304.80	4880.8	307.61	2.81
10.5/320.04	4977.4	319.98	-0.06
11.0/335.28	5026.6	341.25	5.97
11.5/350.52	5098.1	358.32	7.80
12.0/365.76	5195.7	370.49	4.73
12.5/382.00	5315.7	379.48	-2.52
13.0/396.24	5412.4	390.82	-5.42
13.5/411.48	5461.5	412.10	0.62
14.0/426.72	5509.9	433.32	6.60

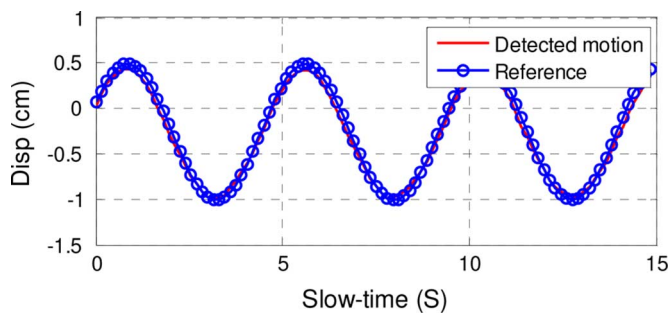

Fig. 8. Comparison between the interferometry-detected displacement and ground truth motion.

B. 2-D Location Mapping

Next, the experiment was moved to real 2-D location and life activities monitoring. The antenna pair was placed at the center of the room and rotated 360° with an angular step size of 5.625°. The room where the experiment was carried out has an octagon shape and is filled with several objects such as sofas, a table, a vending machine, and a trash can. Beside, two people were sitting still and breathing normally in the room. Fig. 9(a) is a panorama photograph depicting the experiment scene. Fig. 9(b) shows the detected and sketched top view of the objects distribution in the room. This map is plotted based on the beat signal alone. The outline of the room is plotted on the map, as well as two people sitting at the 11 o'clock and 9 o'clock directions. The strength of the reflected signal depends on the objects' radar cross section (RCS). The outlines of the room are walls made of strong reflecting materials including solid wood, bricks, and metals. On the other hand, except for some wood frames, the sofas are mainly made of cloth that is a weak reflector. For the vending machine, the majority plastic cover is almost microwave transparent, so only its metal parts are shown on the map. Nevertheless, the good match in location illustrates that the radar shows a decent accuracy in finding the position of each object. Fig. 9(c) shows the actual layout of the room and the distribution of objects in the room, which were measured using a ruler.

C. Vital-Sign Monitoring

At the same time, the rebuilt interferometry signal continuously monitors the movements in the current angular bin.

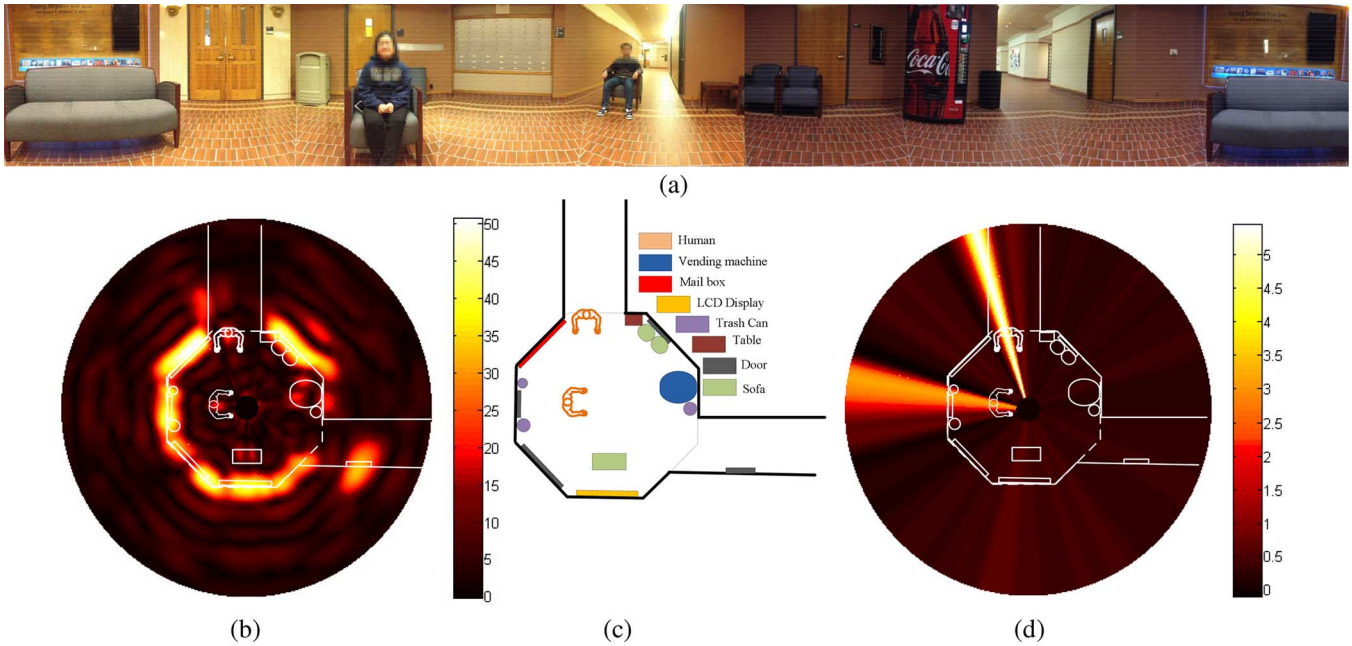

Fig. 9. (a) Panorama photograph of the experiment environment for 2-D positioning and vital sign monitoring. (b) 2-D location map obtained by FMCW detection mode. (c) Room layout and objects distribution in the room. (d) Motion information detected by interferometry mode.

Fig. 9(d) illustrates the angular distribution of motion intensity obtained by the interferometry mode. It should be noted that only the angular direction of targets with motions could be obtained because the interferometry mode is incapable of detecting range. Fig. 10 shows the detected displacements at the 9 o'clock and 11 o'clock directions, respectively. Clear and precise respiration patterns can be observed. The high sensitivity for respiration monitoring is desirable because it can reveal the health condition of the subject being monitored. It is reported that people in different states of health or even in different emotion will show different respiration patterns. Therefore, it is beneficial to not only detect the physiological motion frequency, but also the motion pattern. For example, it has been reported that the movement of thoracic cavity during normal respiration is not restless, but will stop a while after exhilaration [5]. This phenomenon can be clearly observed in both results, especially in Fig. 10(b). According to Taylor expansion with Bessel coefficients, in the spectrum of the detected vital sign signal, higher order harmonics show up because of the sine/cosine phase modulation [27], [28]. When the target is close enough to the radar, it is even possible to monitor the heart beat, as shown in Fig. 10(a).

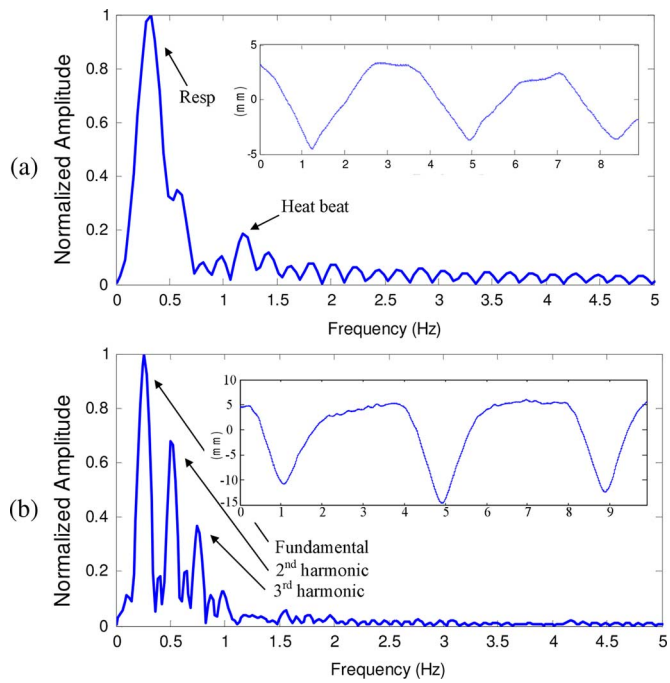

Fig. 10. Measured vital signs from the targets at: (a) 9 o'clock and (b) 11 o'clock, respectively (*insets*) Time-domain waveforms.

D. Stationary Clutters Removal and Target Emphasis

As mentioned in Section II-D, stationary clutter removal should be achieved by the cooperation of interferometry mode and FMCW mode. The FMCW result in Fig. 9(b) is weighted in each angle based on the interferometry signal shown in Fig. 9(d). To minimize the computation load, the background comparison algorithm will only be activated when the amplitude of the displacement detected by the interferometry mode exceeds a threshold. This occurred at the 9 o'clock and 11 o'clock angle in Fig. 9(d). More often than not, the target is not the only object in a given angular bin. Just like the two targets in the experiment of Fig. 9, each human target coexists with other stationary clutters in a given angular bin. Ideally background subtraction algorithm mentioned in Section II-D can eliminate the stationary clutters by taking the first beat signal as a reference and subtract it from the following beat signals in either the frequency or time domains. However, this is risky because beat signals at two moments maybe similar consider the motion is periodic. Therefore, standard deviation of the range spectrum is used in real experiment to differentiate human and stationary target in the same angular direction. Fig. 11 shows the original range spectra of different beat signals. Obviously, the range bins where the moving targets are located have the

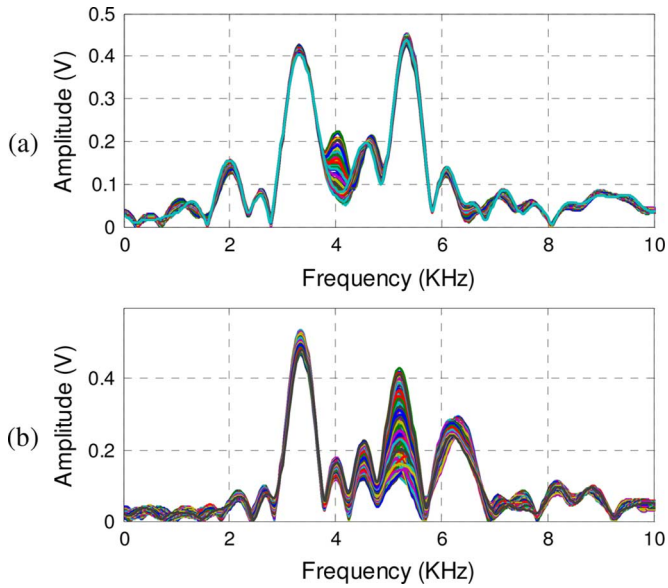

Fig. 11. (a) Range spectra obtained from beat signals at 9 o'clock. (b) Range spectra obtained from beat signals at 11 o'clock.

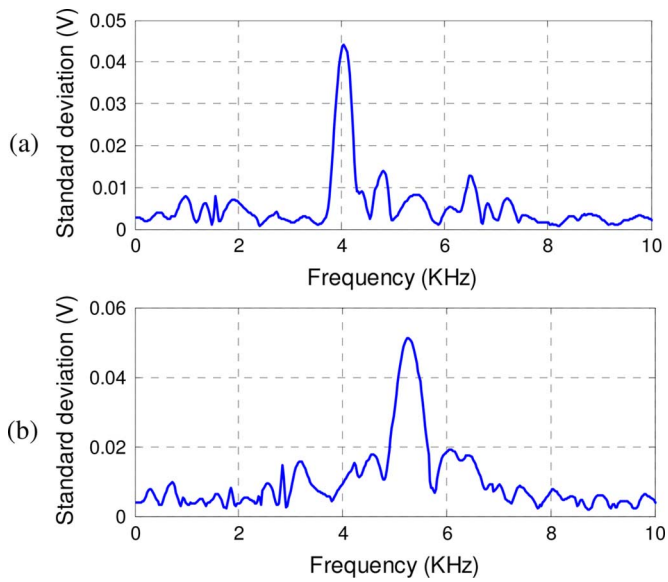

Fig. 12. (a) Standard deviation of the range spectra from beat signals at 9 o'clock. (b) Standard deviation of the range spectra from beat signals at 11 o'clock.

largest variation in amplitude. Fig. 12 demonstrates the standard deviation at each range bin. A larger standard deviation represents a larger movement, which is caused by physiological motion of human subjects. Therefore, the locations with large standard deviations represent the location of human target. Finally, incorporate this algorithm into the previous 2-D map results in a map of human location, as illustrated in Fig. 13, with normalized amplitude. The detected range of the human target at 9 o'clock and 11 o'clock are 1.478 m (versus 1.5 m measured by a ruler) and 3.745 m (versus 3.82 m measured by a ruler), respectively. The reason why the target at 11 o'clock shows a larger RCS than that at 9 o'clock is because the target at 11 o'clock had a larger respiration amplitude. It should be noted that this observation based on the FMCW result agrees well with the respiration measurement result in Fig. 10, which was obtained by the interferometry mode. It was found that the

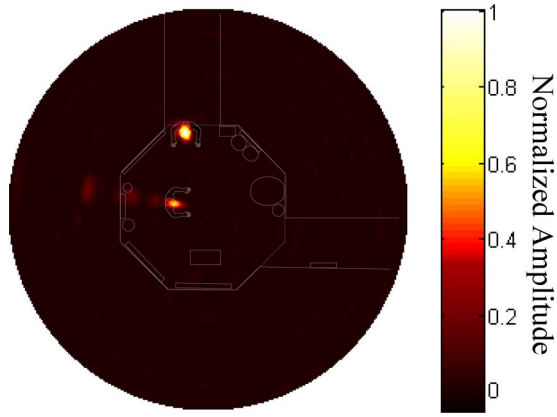

Fig. 13. 2-D map of human targets with stationary clutters removed.

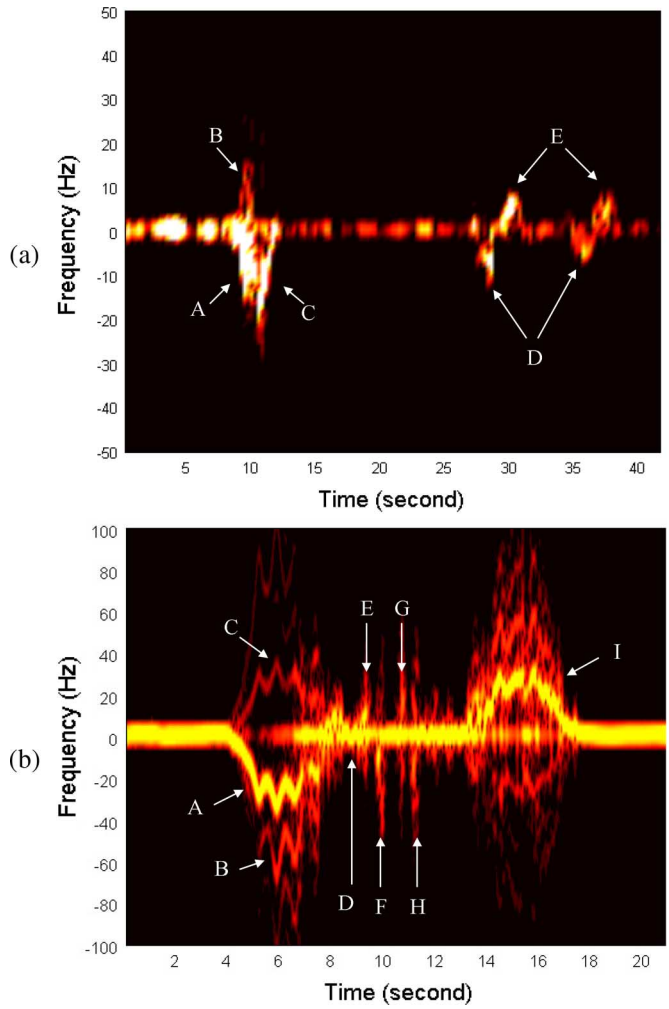

Fig. 14. (a) Micro-Doppler signature of a person sitting down and waving hands twice. (b) Micro-Doppler signature of a walking person.

maximum detection range for the system to localize human targets is around 15 m, which is limited by the signal to noise ratio at the radar receiver output.

E. Micro-Doppler Gesture Recognition

Fig. 14(a) depicts the micro-Doppler information of a series of motions performed by a person facing the radar. The subject changed from standing to sitting on a chair, and then waved his arm twice. When sitting down, most parts of the upper body

moved backward, producing a large negative Doppler frequency component at A. Meanwhile, some other parts such as the head moved forward and created a positive frequency at B. When the bottom reaches the seat, the upper body approaches towards the seatback and creates another significant negative Doppler frequency at C. During the arm-waving action, the subject lifted his arm from the armrest and laid it down immediately, with the elbow serving as the pivot. Correspondingly, on the spectrum there was a negative frequency (D) followed by a positive frequency (E). Between these actions, the target just sat still. Fig. 14(b) describes another series of motion of a subject who walked away from radar, turned around, pushed and pulled the arm twice, and then walked towards radar. When walking away from radar, large negative Doppler frequency can be observed at A, and the ripple came from arm and leg swings. Different parts of arms and legs produce different various Doppler frequency times (B and C). When the subject was turning around, both positive and negative frequency raised simultaneously, yet with smaller values (D), and it is straightforward that the pushing arm produced positive Doppler frequency (E and G) and pulling it back produced negative ones (F and H). When the subject walked towards radar, the Doppler frequency pattern at I is close to a mirrored version at A. With an advanced pattern recognition algorithm, it is possible for computers to recognize certain behaviors and serves as a wireless UI.

IV. Conclusion

A hybrid radar system that integrates the FMCW mode and interferometry mode has been presented. The radar works as a TD system that continuously switches between the FMCW mode and interferometry mode. Basically, the FMCW mode is responsible for absolute range detection and the interferometry mode takes care of weak physiological movement monitoring. Its unique working procedure was first demonstrated using a simulated signal. Experiments have been carried out to validate the accuracy in range detection and displacement measurement. This strategy complements the advantages of the two radar modes so it is able to provide a versatile performance. By steering the antenna beam, the proposed radar system becomes an ideal solution for indoor health care, human localization, and human–computer interaction. Human targets with or without stationary clutters can be precisely located. At the same time, the targets' vital signs and gestures can be monitored. Experimental result showed decent performance of these functions and proved the feasibility of the presented hybrid radar system.

Acknowledgment

The authors would like to acknowledge fruitful discussions with Dr. R. Gómez-García and Dr. J.-M. Muñoz-Ferreras on FMCW radar theory.

References

[1] J. Han, L. Shao, D. Xu, and J. Shotton, "Enhanced computer vision with Microsoft kinect sensor: A review," *IEEE Trans. Cybern.*, vol. 43, no. 5, pp. 1318–1334, Oct. 2013.

[2] C. Li, V. M. Lubecke, O. Boric-Lubecke, and J. Lin, "A review on recent advances in Doppler radar sensors for noncontact healthcare monitoring," *IEEE Trans. Microw. Theory Techn.*, vol. 61, no. 5, pp. 2046–2060, May 2013.

[3] B. Schleicher, I. Nar, A. Trasser, and H. Schumacher, "IR-UWB radar demonstrator for ultra-fine movement detection and vital-sign monitoring," *IEEE Trans. Microw. Theory Techn.*, vol. 61, no. 5, pp. 2076–2085, May 2013.

[4] F. Wang, T. Horng, K. Peng, H. Jau, J. Li, and C. Chen, "Detection of concealed individuals based on their vital signs by using a see-through-wall imaging system with a self-injection-locked radar," *IEEE Trans. Microw. Theory Techn.*, vol. 61, no. 1, pp. 696–704, 2013.

[5] C. Gu, R. Li, H. Zhang, A. Y. C. Fung, C. Torres, S. B. Jiang, and C. Li, "Accurate respiration measurement using DC-coupling continuous-wave radar sensor for motion-adaptive cancer radiotherapy," *IEEE Trans. Biomed. Eng.*, vol. 59, no. 11, pp. 3117–3123, Nov. 2012.

[6] F.-K. Wang, C.-J. Li, C.-H. Hsiao, T.-S. Horng, J. Lin, K.-C. Peng, J.-K. Jau, J.-Y. Li, and C.-C. Chen, "Seeing through walls with a self-injection-locked radar to detect hidden people," in *IEEE MTT-S Int. Mircow Symp. Dig.*, Montreal, QC, Canada, Jun. 2012, pp. 1–3.

[7] Y. Wang, Q. Liu, and A. E. Fathy, "CW and pulse-Doppler radar processing based on FPGA for human sensing applications," *IEEE Trans. Geosci. Remote Sens.*, vol. 51, no. 5, pp. 3097–3107, May 2013.

[8] Y. Kim and H. Ling, "Through-wall human tracking with multiple Doppler sensors using an artificial neural network," *IEEE Trans. Antennas Propag.*, vol. 57, no. 7, pp. 2116–2122, Jul. 2009.

[9] C. Li, X. Yu, C. M. Lee, D. Li, L. Ran, and J. Lin, "High-sensitivity software-configurable 5.8-GHz radar sensor receiver chip in 0.13-μ m CMOS for noncontact vital sign detection," *IEEE Trans. Microw. Theory Techn.*, vol. 58, no. 5, pp. 1410–1319, May 2010.

[10] A. D. Droitcour, O. Boric-Lubecke, V. M. Lubecke, and J. Lin, "0.25-μ m CMOS and BiCMOS single-chip direct-conversion Doppler radars for remote sensing of vital signs," in *IEEE Int. Solid-State Circuits Conf. Tech. Dig.*, Feb. 2002, vol. 1, pp. 348–349.

[11] C. Gu, G. Wang, Y. Li, T. Inoue, and C. Li, "A hybrid radar-camera sensing system with phase compensation for random body movement cancellation in Doppler vital sign detection," *IEEE Trans. Microw. Theory Techn.*, vol. 61, no. 12, pp. 4678–4688, Dec. 2013.

[12] J. C. Y. Lai, Y. Xu, E. Gunawan, E. C. Chua, A. Maskooki, Y. L. Guan, K. S. Low, C. B. Soh, and C. L. Poh, "Wireless sensing of huamn respiratory parameters by low-power ultrawideband impulse radio radar," *IEEE Trans. Instrum. Meas.*, vol. 60, no. 3, pp. 928–938, Mar. 2011.

[13] D. Zito, D. Pepe, M. Mincica, F. Zito, A. Tognetti, A. Lanata, and D. D. Rossi, "SoC CMOS UWB pulse radar sensor for contactless respiratory rate monitoring," *IEEE Trans. Biomed. Circuits Syst.*, vol. 5, no. 6, pp. 503–510, Dec. 2011.

[14] A. Nezirovic, S. Tesfay, A. S. E. Valavan, and A. Yarovoy, "Experimental study on human breathing cross section using UWB impulse radar," in *Proc. 5th Eur. Radar Conf.*, Amsterdam, The Netherlands, Oct. 2008, pp. 1–4.

[15] T. Mitomo, N. Ono, H. Hoshino, Y. Yoshihara, O. Watanabe, and I. Seto, "A 77 GHz 90 nm CMOS Transceiver for FMCW radar applications," *IEEE J. Solid-State Circuits*, vol. 45, no. 4, pp. 928–937, Apr. 2010.

[16] S. Scheiblhofer, S. Schuster, and A. Stelzer, "High-speed FMCW radar frequency synthesizer with DDS based linearization," *IEEE Microw. Wireless Compon. Lett.*, vol. 17, no. 5, pp. 397–399, May 2007.

[17] N. Pohl, T. Jaeschke, and K. Aufinger, "An ultra-wideband 80 GHz FMCW radar system using a SiGe bipolar transceiver chip stabilized by a fractional-N PLL synthesizer," *IEEE Trans. Microw. Theory Techn.*, vol. 60, no. 3, pp. 757–765, Mar. 2012.

[18] J. D. Park and W. J. Kim, "An efficient method of eliminating the range ambiguity for a low-cost FMCW radar using VCO tuning characteristics," *IEEE Trans. Microw. Theory Techn.*, vol. 54, no. 10, pp. 3623–3629, Oct. 2006.

[19] T. Musch, "A high precision 24-GHz FMCW radar based on a fractional-N ramp-PLL," *IEEE Trans. Instrum. Meas.*, vol. 52, no. 2, pp. 324–327, Apr. 2003.

[20] M. Mercuri, P. J. Soh, G. Pandey, P. Karsmakers, G. A. E. Vandenbosch, P. Leroux, and D. Schreurs, "Analysis of an indoor biomedical radar-based system for health monitoring," *IEEE Trans. Microw. Theory Techn.*, vol. 61, no. 5, pp. 2061–2068, May 2013.

[21] Y. S. Su, C. C. Chang, J. J. Guo, and S. F. Chang, "2-D wireless human subjects positioning system based on respiration detections," in *IEEE MTT-S Int. Microw. Symp. Dig.*, Montréal, QC, Canada, Jun. 2012, pp. 1–3.

[22] , M. A. Richards, J. A. Scheer, and W. A. Holm, Eds., *Principles of Modern Radar: Basic Principles*, 2nd ed. Raleigh, NC, USA: SciTech, 2010.
[23] G. Wang, C. Gu, T. Inoue, and C. Li, "Hybrid FMCW-interferometry radar system in the 5.8 GHz ISM band for indoor precise position and motion detection," in *IEEE MTT-S Int. Microw. Symp. Dig.*, Seattle, WA, USA, Jun. 2013, pp. 1–3.
[24] G. Wang, J. M. Munoz-Ferreras, C. Gu, C. Li, and R. Gomez-Garcia, "Linear-frequency-modulated continuous-wave radar for vital-sign monitoring," in *Proc. IEEE Biomed. Wireless Technol., Networks, Sens. Syst. Top. Conf.*, Newport Beach, CA, USA, Jan. 2014, pp. 1–3.
[25] Y. Li, G. Wang, C. Gu, and C. Li, "Movement-immune respiration monitoring using automatic DC-correction algorithm for CW Doppler radar system," in *Proc. IEEE Biomed. Wireless Technol., Networks, Sensing Syst. Top. Conf.*, Newport Beach, CA, USA, Jan. 2014, pp. 7–9.
[26] S. Banerjee, C. Gu, and C. Li, "PXI-based non-contacted vital sign detection system," in *Proc. IEEE Biomed. Wireless Technol., Networks, Sens. Syst. Top. Conf.*, Newport Beach, CA, USA, Jan. 2014, pp. 4–6.
[27] C. Li, Y. Xiao, and J. Lin, "Experiment and spectral analysis of a low-power Ka-band heartbeat detector measuring from four sides of a human body," *IEEE Trans. Microw. Theory Techn*, vol. 54, no. 12, pp. 4464–4471, Dec. 2006.
[28] C. Gu, T. Inoue, and C. Li, "Analysis and experiment on the modulation sensitivity of Doppler radar vibration measurement," *IEEE Microw. Wireless Compon. Lett.*, vol. 23, no. 10, pp. 566–568, Oct. 2013.

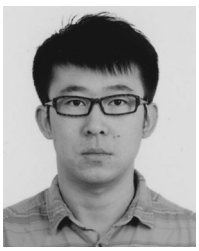

Guochao Wang (S'11) received the B.S. and M.S. degrees in electronics and information engineering from Northwestern Polytechnical University, Xi'an, Shaanxi, China in 2007 and 2010, respectively, and is currently working toward the Ph.D. degree in electrical engineering with Texas Tech University, Lubbock, TX, USA.

He is currently with the Department of Electrical and Computer Engineering, Texas Tech University. His current research interests include microwave/RF wireless sensors, and microwave/millimeter-wave circuit and system design.

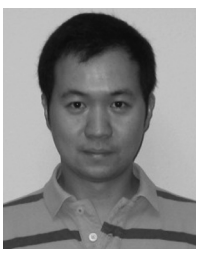

Changzhan Gu (S'07–M'13) received the B.S. and M.S. degrees in information and electronic engineering from Zhejiang University, Hangzhou, China, in 2006 and 2008, respectively, the M.S. degree in electrical engineering from the University of Florida, Gainesville, FL, USA, in 2010, and the Ph.D. degree in electrical engineering from Texas Tech University, Lubbock, TX, USA, in 2013.

From June 2013 to January 2014, he was a Senior RF Systems Engineer with MaxLinear Inc., Irvine, CA, USA, where he was involved with satellite TV tuner systems-on-chip (SoCs). Since January 2014, he has been an Senior Engineer with Marvell Semiconductor Inc., Santa Clara, CA, USA, where he is involved with wireless connectivity technologies. His research interests include RF and microwave circuits/systems, RF systems-on-chip (SoCs), wireless sensing technologies, and the biomedical applications of RF/microwave.

Dr. Gu was the recipient of seven IEEE conference Best Paper Awards as an author/coauthor. As lead author, he was the recipient of Best Paper Awards of IEEE RWW in 2011–2013. He was also the recipient of the IEEE Microwave Theory and Techniques Society (MTT-S) 2013 Graduate Fellowship for Medical Applications, the 2013 Texas Tech Horn Professors Graduate Achievement Award, and the 2012 Chinese Government Award for Outstanding Self-Financed Students Abroad.

Takao Inoue (S'94–M'04) received the B.S. and M.S. degrees in electrical engineering from Oregon State University, Corvallis, OR, USA, in 1996 and 1998, respectively, and the Ph.D. degree in electrical engineering from the University of Texas at Austin, Austin, TX, USA, in 2009.

In 1998, he joined Motorola Inc., where he was involved with ADSL modem development and ITU standardization for G.DMT. In 2004, he became a consultant involved with an FPGA-based signal processing accelerator for wireless applications and became the co-founder and Chief Technical Officer (CTO) of Fish Technologies Inc., which specialized in advanced wireless system prototyping. Since 2010, he has been with National Instruments, Austin, TX, USA, where he has been involved with wireless system prototype development, 3GPP standardization activities, and RF/microwave systems research. His research interest includes signal processing and mathematics for wireless communications systems and related circuits and systems implementation.

Dr. Inoue has served on the Steering Committee of the IEEE Radio Frequency Integrated Circuits Symposium (2001–2013) and the IEEE Radio and Wireless Symposium (2004–2014). He was the recipient of the 2004 IEEE Microwave Theory and Techniques Society (IEEE MTT-S) Meritorious Service Award.

Changzhi Li (S'06–M'09–SM'13) received the B.S. degree in electrical engineering from Zhejiang University, Zhejiang, China, in 2004, and the Ph.D. degree in electrical engineering from the University of Florida, Gainesville, FL, USA, in 2009.

In the summers of 2007–2009, he was with Alereon Inc. Austin, TX, USA, and Coherent Logix Inc. Austin, TX, USA, where he was involved with ultra-wideband (UWB) transceivers and software-defined radio. In 2009, he joined Texas Tech University, Lubbock, TX, USA, as an Assistant Professor, and became an Associate Professor in 2014. His research interests include biomedical applications of microwave/RF, wireless sensor, and RF/analog circuits.

Dr. Li is an associate editor for the IEEE TRANSACTIONS ON CIRCUITS AND SYSTEMS—II: EXPRESS BRIEFS. He was an area editor for the *International Journal of Electronics and Communications* (2011–2013). He was the Technical Program Committee (TPC) co-chair for the IEEE Wireless and Microwave Technology Conference (WAMICON) (2012 and 2013). He was the recipient of the ASEE Frederick Emmons Terman Award, the IEEE-HKN Outstanding Young Professional Award, and the Texas Tech Whitacre Research Award in 2014. He was the recipient of the National Science Foundation (NSF) Faculty Early CAREER Award (2013), the Texas Tech Alumni Association New Faculty Award (2012), and the IEEE Microwave Theory and Techniques Society (IEEE MTT-S) Graduate Fellowship Award (2008). He was also the recipient of nine Best Conference/Student Paper Awards as an author/advisor of the IEEE Radio and Wireless Week (RWW) and IEEE WAMICON.